



# Green method for preparation of cellulose nanocrystals using deep eutectic solvent

Michael A. Smirnov · Maria P. Sokolova · Dmitry A. Tolmachev · Vitaly K. Vorobiov · Igor A. Kasatkin · Nikolay N. Smirnov · Anastasya V. Klaving · Natalya V. Bobrova · Natalia V. Lukasheva · Alexander V. Yakimansky

Received: 10 September 2019 / Accepted: 8 March 2020 / Published online: 21 March 2020  
© Springer Nature B.V. 2020

**Abstract** An environment-friendly method for obtaining cellulose nanocrystals (CNC) using deep eutectic solvents (DES) was developed. Formation of highly crystalline CNC with average particle dimensions  $20 \times 100 \times 700$  nm was confirmed with SEM and AFM. Molecular dynamics simulations demonstrated that the hydrogen bond interactions of the cellulose hydroxyl groups with the urea C=O group

and with the chloride ions were the key factors of the destruction of MCC particles in the process of solvation. The type of cellulose crystal structure ( $I_{\beta}$ ) and the high degree of crystallinity (about 80% according to Segal method) were preserved during treatment with DES. The ability of the prepared CNC to act as a reinforcing filler was tested by introduction of them into the chitosan-based films plasticized with DES. It was found that addition of 2 wt% of CNC led to an increase in the strength of the films from 11.4 up to 20.4 MPa with a simultaneous increase in the elongation at break.

**Electronic supplementary material** The online version of this article (<https://doi.org/10.1007/s10570-020-03100-1>) contains supplementary material, which is available to authorized users.

M. A. Smirnov (✉) · M. P. Sokolova · D. A. Tolmachev · V. K. Vorobiov · N. N. Smirnov · N. V. Bobrova · N. V. Lukasheva · A. V. Yakimansky  
Institute of Macromolecular Compounds,  
Russian Academy of Sciences, Bolshoy pr. 31,  
Saint Petersburg, Russia 199004  
e-mail: smirnov\_michael@mail.ru

M. P. Sokolova  
e-mail: pmarip@mail.ru

D. A. Tolmachev  
e-mail: dm.tolmachev@yandex.ru

V. K. Vorobiov  
e-mail: vrbvrbvrb@mail.ru

N. N. Smirnov  
e-mail: rambow@inbox.ru

N. V. Bobrova  
e-mail: bobrovanatalialab19@mail.ru

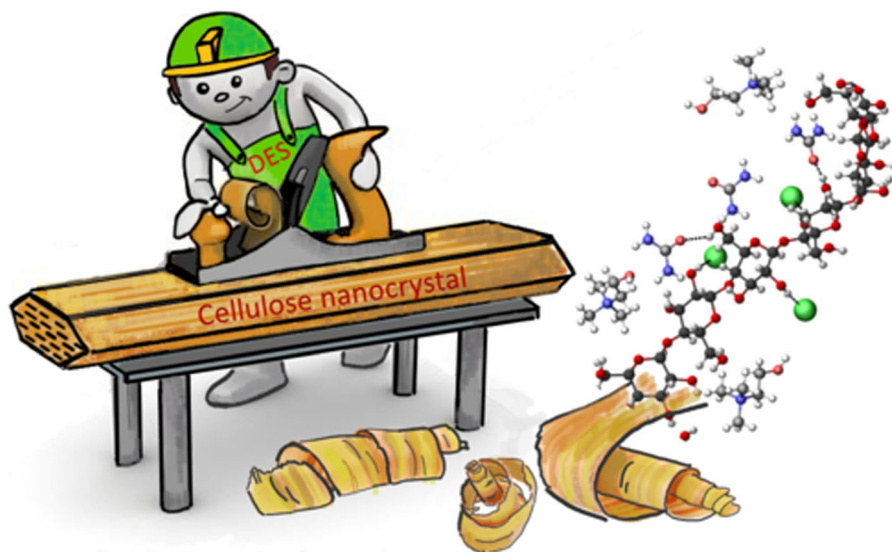
N. V. Lukasheva  
e-mail: luk@imc.macro.ru

A. V. Yakimansky  
e-mail: yak@hq.macro.ru

I. A. Kasatkin · A. V. Klaving  
Saint Petersburg State University,  
Universitetskaya Emb. 7-9, Saint Petersburg,  
Russia 198504  
e-mail: igor.kasatkin@spbu.ru

A. V. Klaving  
e-mail: 8330215@gmail.com

## Graphic abstract



**Keywords** Cellulose nanocrystals · Chitosan · Deep eutectic solvent · Reinforcing · Molecular dynamics simulation

## Introduction

Due to unique combination of properties, such as large specific surface area, high tensile strength and stiffness, the cellulose nanomaterials can be used as reinforcing fillers for polymer films (Deng et al. 2017; Cao et al. 2018; Surov et al. 2018a; Ying et al. 2018), templates for preparation of functional (Wang et al. 2018) and stimuli-responsive materials (Feng et al. 2014; Tang et al. 2016), sensors (Wu et al. 2015; Li et al. 2018) or electrochemically active materials (Armelin et al. 2016; Smirnov et al. 2018). Additionally, cellulose is the most abundant renewable polymer, and its application meets the requirements of sustainable and green technology.

High crystallinity and a strong network of hydrogen bonds between the chains complicate processing of cellulose. Hydrolysis of amorphous regions with concentrated inorganic acids (Mondal 2017) has long been the most common process for preparation of cellulose nanocrystals (CNC) and nanofibers. Recently other methods, such as enzymatic hydrolysis (Rovera et al. 2018), TEMPO-mediated (Hirota et al.

2010; Zhou et al. 2018) or ammonium persulfate (Leung et al. 2011) oxidation, plasma treatment (Surov et al. 2018b) and processing with ionic liquids (ILs) (Miao et al. 2016) were also proposed. Some of those methods are complicated while the hazardous chemicals are needed for others. For example, the mineral acids and some types of ILs are not safe for the environment. Enzymatic hydrolysis needs enzymes used under special conditions, and as plasma treatment needs special equipment. Cellulose nanomaterials can be prepared via a non-oxidative and non-hydrolytic dissolution with subsequent regeneration (Man et al. 2011; Li et al. 2012) utilizing the IL's ability to broke intramolecular hydrogen bonds. However, the high cost and the toxicity of the majority of traditional ILs (Amde et al. 2015; Troter et al. 2016) restrict their wide practical application.

Deep eutectic solvents (DES) present a new and prospective alternative for ILs. DES demonstrate the same beneficial physico-chemical properties while being cheaper than ILs and preparable from more simple natural green components (Zhang et al. 2012). Abilities of DES to act as media for processing various biomasses, including cellulose, have recently been under intensive investigation (Ren et al. 2016; Suopajarvi et al. 2017; Zainal-Abidin et al. 2017; Zhu et al. 2017). DES are capable of preferential dissolving lignin from loblolly pine that increases the glucose yield during subsequent enzymatic hydrolysis

(Lynam et al. 2017); they can effectively extract bioactive molecules—for example, isoflavones—from soy product (Bajkacz and Adamek 2017). Typically, DES consist of a hydrogen bond donor and an acceptor which interact strongly with each other. As a result, an eutectic mixture with a melting point below that of both initial components is formed (Smith et al. 2014). The ability to form a strong network of hydrogen bonds allows DES to interact with various molecules and polymers via hydrogen bonding, that makes DES useful either as selective sorbents for liquid–liquid extraction (Samarov et al. 2018a, b) or as a new type of plasticiser for the polysaccharide based films (Galvis-Sánchez et al. 2016; Decaen et al. 2017; Sokolova et al. 2018). This ability also allows for effective solubilization and dissolution of some natural polysaccharides (Mukesh et al. 2014; Liu et al. 2017). However, DES were mainly used only for the pretreatment of cellulose prior to the preparation of nanoparticles by other methods (Sirviö et al. 2016; Suopajarvi et al. 2017). No information is available on the possibility of direct DES application for the preparation of cellulose nanomaterials. It was reported recently that treatment of pine pulp with choline chloride—urea (ChCl/Ur) deep eutectic mixture during 16 hours at 100 °C did not influence the pulp fiber morphology (Tenhunen et al. 2018). At the same time, changing of morphology of cotton fibers at treatment with choline chloride—oxalic acid DES simplifies the subsequent CNC preparation using ultrasound (Ling et al. 2019). Possibly, DES is not active enough to solubilize the non-treated plant cellulose because of the cooperative effect of multiple intermolecular hydrogen bonds. If that is a significant reason, then one can expect a higher probability of successful splitting into nanomaterial for the cellulose of smaller molecular mass. Thus, the aim of this work was to investigate the possibility of CNC preparation using DES from the commercially available microcrystalline cellulose (MCC). Its high crystallinity index allows obtaining CNC without a pretreatment stage of amorphous regions removal in cellulose. Recent studies showed that CNC could be obtained by chemical treatment of MCC by hydrolysis in H<sub>2</sub>SO<sub>4</sub> solution (Bai et al. 2009; dos Santos et al. 2017) or by TEMPO oxidation (Zhou et al. 2018). High-energy bead milling (Amin et al. 2015) can also be used for transforming MCC into CNC. At the same time, the ability of DES to destruct MCC particles and to form a

cellulose nanomaterial was not tested yet. The mixture of ChCl and Ur was chosen as one of the most capacitive ones towards dissolution of cellulose according to the literature data (Ren et al. 2016). The CNC prepared here were tested as reinforcing fillers for chitosan (CS) films plasticized with DES.

## Experimental part

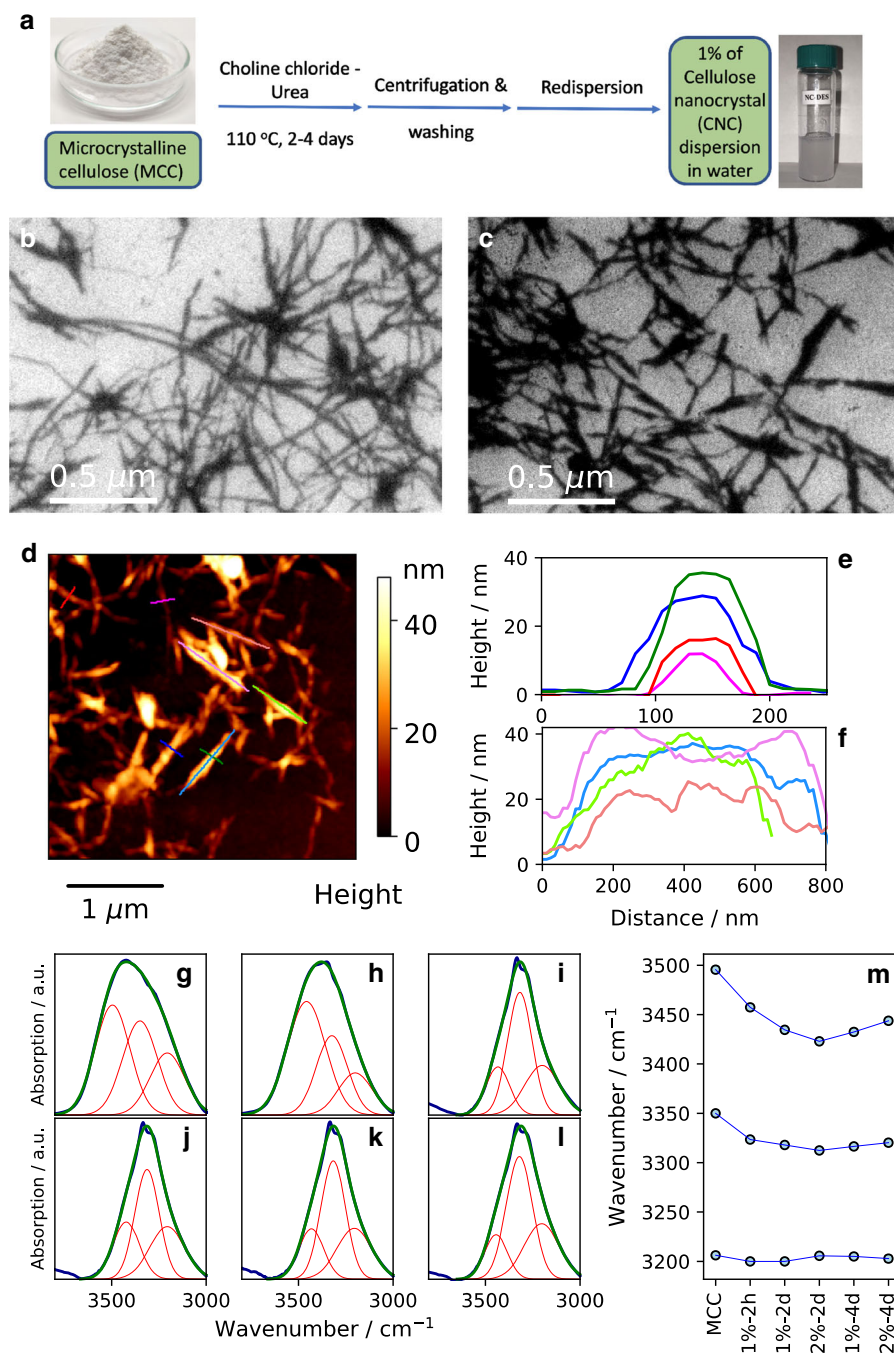
### Materials

The following starting materials were used in the experiments: ChCl (Acros Organics, China); Ur purchased from LKB BROMMA (Bromma, Sweden); malonic acid (Vecton, Russia); MCC (Sigma-Aldrich, USA); CS with the  $M_w = 900\,000$  and the degree of deacetylation of DA = 68% (“Bioprogress CJSC”, Russia).

### Preparation of CNC from MCC

The DES (5 g) was prepared by mixing ChCl (2.71 g) and Ur (2.32 g) at 60 °C in a flask immersed in the oil bath equipped with a magnetic stirrer and a calcium chloride tube. After the formation of a viscous liquid, the MCC (1 or 2 wt%) was added and the temperature was raised up to 110 °C and kept for 2 or 4 days. The resulting suspension was cooled down, mixed with 10 ml of deionized water and centrifuged at 4000 rpm for 10 min. The precipitate was further redispersed by manual mechanical stirring in 10 ml of deionized water. The centrifugation and redispersion steps were repeated three times. The scheme of preparation of CNC dispersion in water is shown in Fig. 1a. The CNC prepared with different concentrations of MCC (1 and 2 wt%) and different duration of treatment [2 hours (2h), 2 days (2d) or 4 days (4d)] were named 1%-2h, 1%-2d, 1%-4d, 2%-2d and 2%-4d, respectively. The sample with 1% of MCC treated for 2 hours was prepared to visualize the process of MCC destruction (see Electronic Supplementary Information (ESI), Fig. S1). The yield of CNC was calculated from the concentration ( $x(\text{CNC})$ ) of the dispersion of final product as  $\text{Yield} = x(\text{CNC}) \times M/m$ , where  $M$  is the overall mass of the dispersion obtained and  $m$  is the mass of the initial MCC. The value of  $x(\text{CNC})$  was found by drying of 1 g of dispersion at 110 °C until the constant weight was reached. A comparison of the

**Fig. 1** Scheme of preparation of CNC dispersion (a); SEM images of CNC prepared in DES during 2 (b) and 4 (c) days; AFM surface topography of 2%-4d (d) and profile curves of CNC in perpendicular (e), and longitudinal (f) directions; the fitting of FTIR spectra in the region  $3600\text{--}3000\text{ cm}^{-1}$  with three Gaussian peaks for initial MCC (g), 1%-2h (h), 1%-2d (i), 2%-2d (j), 1%-4d (k), 2%-4d (l) and positions of peak maxima (m)



yield and characteristics of our process with other methods for preparation of CNC from MCC are given in ESI, Table S1. Zeta potential of CNC in the dispersion was measured using Zetasizer Nano ZS with He–Ne laser ( $\lambda = 633\text{ nm}$ ; Malvern Instruments, Worcester, UK) at  $25\text{ }^{\circ}\text{C}$ . The molecular mass ( $M_n$ ) of

cellulose in MCC and CNC was determined from the characteristic viscosity of a cellulose solution in iron(III) sodium tartrate complex using the equation  $[\eta] = 5.31 \times 10^{-4} M_n^{0.73}$  (Kabanov 1977).

## Preparation of plasticized CS reinforced with CNC

The CS films plasticized with a mixture of malonic acid (MA) and ChCl (Sokolova et al. 2018) were prepared by solution casting method with various CNC contents. Typically, 0.66 g CS, 0.767 g ChCl and 0.573 g MA dry powders were added in a flask containing 100 ml of distilled water. Four solutions with the same CS, ChCl and MA content were stirred for 6 days at room temperature (20–25 °C) until CS was completely dissolved. The solutions were filtered to remove undissolved residual and degassed under vacuum. Afterwards, various amounts of the homogeneous water dispersion with 1 wt% of CNC (sample 1%-2d) were added in flasks containing the CS-DES solutions. The masses of the added CNC dispersions were 4, 8 and 12 g, respectively. Solutions were stirred for 5 h for better distribution of the CNC. The films with the thickness of 20 µm were prepared by solution casting method on a glass surface with subsequent drying at 25 °C for 6 days. The CNC concentrations were 2, 4 and 6 wt%, respectively.

## Characterization methods

### *Microscopy investigations*

The morphologies of the MCC, CNC and the reinforced films were studied with a scanning electron microscope Zeiss AURIGA Laser (Carl Zeiss, Germany). The atomic force microscopy (AFM) was performed with an INTEGRA-AURA microscope (NT-MDT, Russia).

### *Fourier-transform infrared spectroscopy*

The chemical structure of the prepared samples was characterized with transmission Fourier-transform infrared spectroscopy (FTIR) with a Nicolet 8700 spectrometer (Thermo Scientific, USA) in the range of 4000–500 cm<sup>-1</sup>. The spectra were measured for the as synthesized samples in the transmittance mode using KBr pellets with the resolution of 2 cm<sup>-1</sup>.

### *Wide-angle X-ray diffraction*

Wide-angle X-ray diffraction (WAXD) study was performed with a D8 Discover diffractometer (Bruker,

Germany) equipped with a CuK<sub>α</sub> radiation source (λ = 1.54 Å).

The degree of crystallinity was estimated by the Segal peak height method (Segal et al. 1959).

The following equation was used:

$$\chi_S = \frac{I_{200} - I_{\min}}{I_{200}}, \quad (1)$$

where  $I_{200}$  and  $I_{\min}$  are the intensity of the  $I_{\beta}$  cellulose (200) diffraction peak located at  $2\theta = 22.5^\circ$  and the background intensity in the region of  $2\theta = 18^\circ$ – $19^\circ$ , respectively.

The average size of crystallites was estimated using the Scherrer equation:

$$L_{hkl} = \frac{K\lambda}{\beta_{hkl} \cos\theta}, \quad (2)$$

where  $L_{hkl}$  is the crystallite size in the direction perpendicular to the lattice plane  $hkl$ ,  $K = 0.94$  is the Scherrer constant,  $\lambda$  is the wavelength of X-rays (1.54 Å),  $\beta_{hkl}$  is the full width at the half-maximum of the corresponding  $hkl$  peak in radians, and  $\theta$  is the Bragg angle.

According to (French and Santiago Cintrón 2013), the Segal method underestimates of the crystallinity index because the scattering in the region of  $2\theta = 18^\circ$ – $19^\circ$  also contains some signal from the “tails” of the crystalline peaks, especially when the crystallite size is small. A full profile refinement by Rietveld method or WPPM (Whole Powder Pattern Modelling), was also performed in this work. This approach does not presume a certain XRD peak shape (strictly Gaussian, Lorentzian, etc.). The peak shape may vary according to the crystallite size, the distribution width and the presence of microstrain. More precisely, what is measured is not the mean crystallite size, but the mean elementary column length. Every single particle of a certain shape is built of elementary columns of different length, thus producing a length distribution that is “convoluted” with the particle size distribution. When the final distribution is sufficiently wide, the diffraction peaks have long “tails” (slow decay of diffracted intensity from the maximum to the background). The overlapping tails of the wide (due to small coherent length) neighboring peaks make the minimum intensity in the “valleys” between them always higher than the real background intensity. This effect may produce an impression that an amorphous phase is present.



Modelling of the XRD patterns of CNC with the TOPAS 5.0 (Bruker) software results in good fits (Fig. S2 in ESI is an example) without considering an amorphous material as a separate phase in our samples. Instead, what is typically regarded as an amorphous phase is included in the single-phase model as a part that consists of the smallest crystallites, which can even be smaller than a unit cell. In a continuous size distribution function, there is no sharp border between the materials with different mean crystallite sizes.

With this approach, it is the whole distribution function that must be analyzed, not just the mean size or length, which can be the same for different distribution functions. A detailed analysis of the distribution functions was outside the scope of this work. Here we limited ourselves to the well-known method for crystallinity analysis.

#### *Molecular dynamics simulation of the cellulose-DES interactions*

Two systems were considered for the simulation: (1) pure deep eutectic solvent (DES) for the validation of the simulation parameters, and (2) DES on the (100) surface of a cellulose crystal, which is the most pronounced surface plane of a cellulose fiber. The cellulose surface was infinite by periodic boundary condition in two directions and formed by 64 chains consisting of 16 glucose residues. A snapshot of the equilibrated simulation box is shown in Fig. S3. Each system included 1310 urea molecules, 655 choline molecules and chloride ions. The constant temperature was maintained by the Nosé–Hoover thermostat (Nosé 1984; Hoover 1985) and the pressure coupling was done isotropically using the Parrinello–Rahman barostat (Parrinello and Rahman 1981) with the coupling times of  $\tau_T = 1$  ps and  $\tau_P = 5$  ps, respectively. Long-distance Coulomb interactions were taken into account by using the PME method (Essmann et al. 1995). The time step was 0.001 ps.

For all of the compounds the models based on OPLS-AA force field were used. For the ChCl molecule the model developed by Sambasivarao and Acevedo (2009) was used. Ur was modelled according to Weerasinghe and Smith (2003). This model showed a good agreement with experiment (Sun et al. 2013) in the simulation of ChCl/Ur mixtures. OPLS-AA force field for carbohydrates was used for cellulose (Kony

et al. 2002). The simulations were performed with the program package Gromacs 5.1.4 (Abraham et al. 2015).

The compounds were added to the simulation box as a molecular gas. The preliminary simulation was performed in several steps. First, the initial systems with the molecular gas were compressed during 2 ns by a pressure of 5 bar. In order to obtain an equilibrium structure, the simulations were performed at  $T = 600$  K,  $P = 1$  bar. The final configurations were then sequentially cooled to 383 K as described in Table S2. The simulation results were validated by comparing the simulated and experimental values of DES density and of diffusion coefficients of its components. Additional details of the simulation cell preparation and the results of validation are given in ESI (“Validation of molecular dynamics simulation” section, Fig. S3–S6).

#### *Mechanical measurements of the films reinforced with CNC*

The mechanical properties (tensile strength, Young’s modulus and elongation at break) of the reinforced films were measured in tensile mode with a UMIV-3 mechanical testing machine (Ivanovo, Russia). The ASTM D882 standard was used to determine the mechanical properties based on at least 10 measurements for each sample using stripes with size  $20 \times 2$  mm and speed  $5 \text{ mm min}^{-1}$ .

## Results and discussion

### Preparation of CNC

Scanning electron microscopy (SEM) images demonstrate a destruction of MCC: from initial particles (Fig. S1a) through partially destroyed particles after 2 hours of treatment (Fig. S1b) to the CNC after 2 and 4 days (Fig. 1b and c, respectively). The initial MCC had short rod-like particles with a diameter of about 20  $\mu\text{m}$  and a length of about 60–100  $\mu\text{m}$  (Fig. S1a). After 2 days the CNC with 80–120 nm thickness and the length of up to several microns were formed (Fig. 1b). Increasing treatment time up to 4 days led to a noticeable decrease in the CNC length (Fig. 1c). No effect of the MCC concentration on the morphology was observed. Accurate measurements with AFM (Fig. 1d, e

and f, respectively) demonstrate the average sizes of CNC of  $20 \times 100 \times 700$  nm in the samples prepared in 4 days (in our case that was the maximum degree of the MCC splitting). Obtained CNC dispersions in water were stable for at least 1 month.

According to the viscometry measurements the degree of polymerization of initial MCC (DP = 330) does not change during the treatment with DES for all type of CNC. In agreement with literature data (Sirviö et al. 2015) there was no hydrolytic destruction of cellulose chains under applied conditions.

The thermal stability of the prepared CNC was studied using thermogravimetric analysis (TGA). The experimental details are given in ESI “Results and discussion” section and the results are shown in Fig. S7a and b. The thermal properties of CNC were independent of the preparation conditions. The decomposition temperatures of MCC and CNC were 290 °C and 251 °C, respectively. Differential scanning calorimetry (Fig. S7c) demonstrated a single endothermic peak at about 60 °C, associated with water desorption from the cellulose. A low surface potential of  $-7$  to  $-13$  mV proves a small degree of surface modification. This is in conflict with the colloidal stability of the prepared CNC. Probably, a large number of -OH groups appear on the surface of CNC due to strong interaction with DES. Those -OH groups form hydrogen bonds with water during washing and make the CNC surface hydrophilic. The shell of tightly bonded water molecules prevents CNC from fast agglomeration.

### FTIR study

The FTIR spectra of the initial MCC and CNC samples are shown in Fig. S8. The peaks in the range of  $700$ – $1500$   $\text{cm}^{-1}$  are typical of cellulose; they do not change upon treatment with DES indicating stability of the cellulose chemical structure. The most apparent changes are seen in the region of  $1700$ – $1600$   $\text{cm}^{-1}$ . A decreased adsorption near  $1620$   $\text{cm}^{-1}$  can be attributed to the removal of the bounded water during prolonged ( $\approx 2$  days) treatment at  $110$  °C. Appearance and further increase in the peak intensity at  $1710$   $\text{cm}^{-1}$  gives evidence for a possible oxidation of the  $\text{C}_6$  cellulose atom with the formation of carboxylic groups. This suggestion is supported by the CNC zeta potential of  $-7$  to  $-13$  mV. A significant change is observed in the shape of the absorption peak at  $3000$ – $3600$   $\text{cm}^{-1}$

which corresponds to the -OH group vibrations. This band was fitted with three peaks centred near  $3500$ – $3450$ ,  $3320$  and  $3210$   $\text{cm}^{-1}$  (Fig. 1g–m) which were attributed to the weakly hydrogen-bonded OH groups, strongly hydrogen-bonded OH groups, and  $\text{O}_2$ -H groups bonded with  $\text{O}_6$ , respectively (Maréchal and Chanzy 2000; Lee et al. 2015). The band near  $3500$ – $3450$   $\text{cm}^{-1}$  demonstrates a red shift, and its intensity decreases (Fig. 1m). Less pronounced red shift is also noticeable for the band near  $3320$   $\text{cm}^{-1}$ , while the band near  $3210$   $\text{cm}^{-1}$  remains in the same position (Fig. 1m). The red shift can be attributed to the increase in the amount of OH groups incorporated into hydrogen-bonding. The decreasing intensity of the band associated with the free OH groups also suggests an increasing amount of the hydrogen-bonded OH groups. Thus, the cellulose molecules which are less incorporated into the hydrogen-bond network are preferably dissolved during treatment with DES.

### WAXD study

The WAXD results show that both CNC and the original MCC have the same typical crystal structure of cellulose  $\text{I}_\beta$  (French 2014) with the characteristic diffraction peaks 1–10, 110, 102 and 200 at  $2\theta = 14.9^\circ$ ,  $16.5^\circ$ ,  $20.7^\circ$  and  $22.5^\circ$ , respectively (Fig. 2). The degree of crystallinity determined by the Seagal method does not change significantly

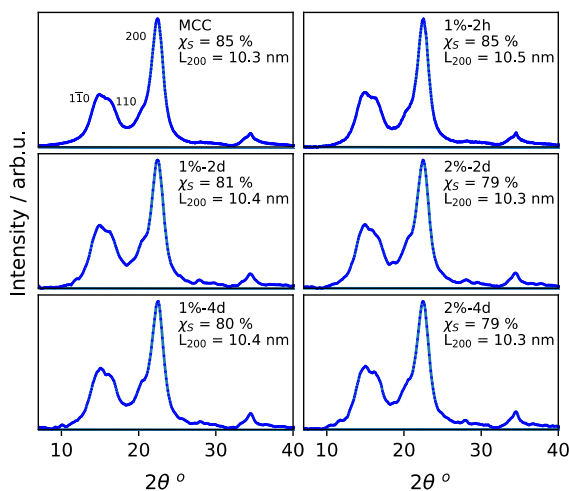


**Fig. 2** X-ray diffraction patterns for MCC and CNC produced under different conditions.  $\chi_s$  is the degree of crystallinity calculated according to the Seagal method.  $L_{200}$  is the size of crystallites in the [100] direction

during treatment with DES, and the average size of crystallites ( $L_{200}$ ) remains approximately the same (Fig. 2). A full profile refinement qualitatively leads to the same result: the degree of crystallinity is very high (close to 100%), and it does not change upon treatment with DES. This suggests that the crystalline regions were not highly affected during the MCC treatment with DES.

### Molecular dynamics simulation results

DES is a multicomponent solvent, and both ChCl and Ur can form hydrogen bonds with the hydroxyl groups of a cellulose molecule. Moreover, both of the components can interact with cellulose via a chloride ion which can be adsorbed on the cellulose molecule due to ion–dipole interaction. It is not clear, which interactions are responsible for the cellulose dissolution. To get insight into this problem, molecular dynamics (MD) simulation of the cellulose surface in DES was performed. A snapshot illustrating the interactions and the radial distribution functions (RDF) between the atoms of cellulose, hydroxyl groups and the atoms of DES components are shown in Fig. 3a. The RDF were computed for two cases: (1) interactions with the secondary –OH groups of cellulose in which cellulose acts as a hydrogen bond acceptor or donor (Fig. 3b, c, respectively); (2) interactions with the primary –OH groups of cellulose in which cellulose acts as an acceptor or donor (Fig. 3d, e, respectively). Well pronounced peaks are observed in RDF functions in Fig. 3c, e for the H atoms of cellulose with the O atoms of Ur and with the  $\text{Cl}^-$  ions. This result is in agreement with the simulation of a cellulose fibril in 1-butyl-3-methylimidazolium chloride (Mostofian et al. 2014), which also shows an importance of chloride ions in the process of the cellulose dissolution. An ion–dipole interaction is stronger than an interaction between two dipoles. At the same time, the ion–dipole interactions between the cellulose hydroxyl and the choline trimethylamine groups are not favourable (Fig. 3b, d) because of the large size of the trimethylamine group, that hampers the interaction sterically.

It is important to mention that the RDF peak is higher for secondary hydroxyl groups than for the primary groups. This contradicts the simulation results published for the cellulose crystals in water environment (Lukasheva and Tolmachev 2016; Kostritskii

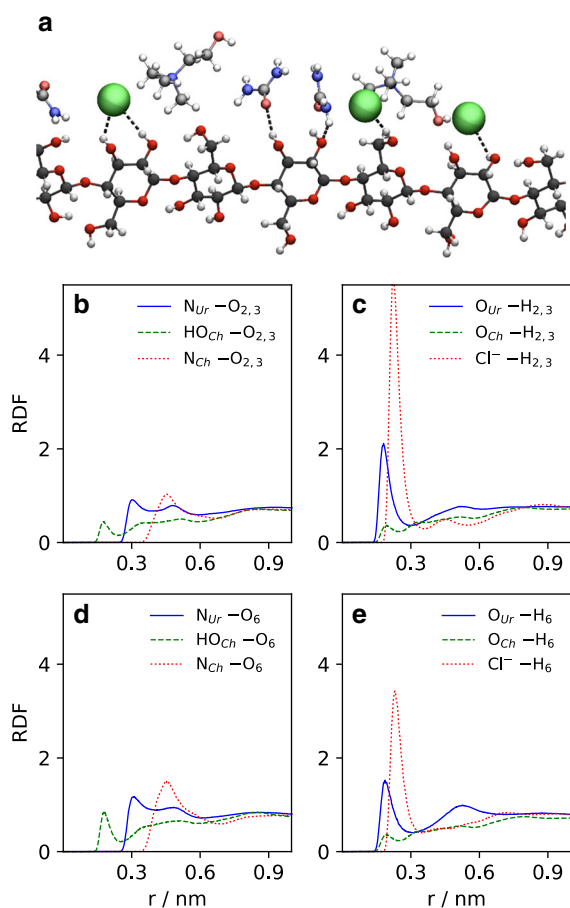


**Fig. 3** Snapshot representing the interaction between cellulose, chloride ions and Ur molecules (a); radial distribution functions between  $\text{O}_{2,3}$  (b),  $\text{H}_{2,3}$  (c),  $\text{O}_6$  (d) and  $\text{H}_6$  (e) atoms of cellulose and choline (Ch), urea (Ur) and chloride ions ( $\text{Cl}^-$ ) from DES. A single cellulose molecule and a few DES molecules which are interacting with cellulose are shown. Red balls represent oxygen atoms, blue balls—nitrogen atoms, white balls—hydrogen atoms, grey balls—carbon atoms and green balls—chloride ions

et al. 2017). In water, the primary hydroxyl groups interact stronger with the external environment because the secondary hydroxyl groups are located deeper in the cellulose surface layer, and they form intramolecular H-bonds. Due to a low dielectric constant of DES (in contrast to water), ion–dipole interaction becomes energetically more favorable than the H-bonding. Moreover, location of the secondary hydroxyl groups close to each other makes it possible to adsorb a  $\text{Cl}^-$  ion by two groups simultaneously. This produce a difference between the intensities of RDF maxima for the primary and secondary hydroxyl groups (see Fig. 3). The destruction of the H-bonds is a



direct evidence of the DES ability to solubilize cellulose macromolecules.

#### Reinforcement of the plasticized CS films with CNC

The possibility of application of the prepared CNC as reinforcing fillers was tested with CS films plasticized with DES. The initial films based on CS, ChCl and MA were prepared and investigated in our previous work (Sokolova et al. 2018). In this work these films were reinforced with 2, 4 and 6 wt% of CNC (sample 1%-2d); the corresponding samples are denoted as CS/CNC-2, CS/CNC-4 and CS/CNC-6, respectively. The reference film prepared without addition of CNC is named CS/CNC-0.

SEM images of the cross-sections of CS/CNC-0 and of the film containing 2 wt% CNC are shown in Fig. 4a, b, respectively. It is seen that the cross-section of CS/CNC-0 is smooth, while that of the CS/CNC-2 film is rougher, illustrating the influence of CNC on the fracture process. No agglomeration of CNC inside the films was observed (Fig. 4b). The effect of the CNC content on the mechanical properties of the composite films (Young's modulus, strength and elongation at break) was tested in the uniaxial tension

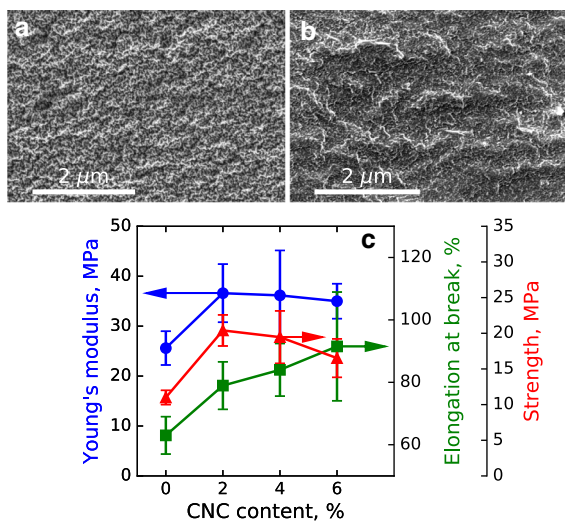


**Fig. 4** SEM images of the cross-section of unmodified film (CS/CNC-0) (a) and of the film containing 2 wt% of CNC (b); dependences of the Young's modulus (circles), elongation at break (squares) and strength (triangles) of the plasticized chitosan films on the CNC content (c): the arrows show the direction toward Y axis containing values for given curves

mode. The results (Fig. 4c) show that incorporation of 2 wt% of CNC leads to an increase in the average strength from 11.4 MPa (for CS/CNC-0) up to 20.4 MPa. The elongation at break and the Young's modulus also increase from 63 up to 79% and from 26 up to 37 MPa, respectively. Thus, the incorporation of CNC leads to an increase in strength by 79% and in elongation at break by 25%.

Recently, a 40% increase in strength was demonstrated for the CS films reinforced with CNC and prepared via an acid hydrolysis procedure (Chi and Catchmark 2018). This result was obtained for a CS film without a plasticizer, thus the elongation at break was only 1.7% and 2.4% for the pristine and reinforced CS, respectively. In another example of CS reinforcement with CNC prepared via acetic acid hydrolysis the tensile strength and the elongation at break increased by 13.2% and 56.4%, respectively (Mao et al. 2019). A 44.2% increase in strength without a change in the elongation at break was also reported recently (Marín-Silva et al. 2019) for the CS reinforced with CNC. Thus, the increase in elasticity observed in our work is moderate, while the growth in strength is approximately two times higher compared with the reported analogues.

The WAXD patterns (Fig. 5a) demonstrate an increase in the intensity of the crystalline peaks with an addition of CNC. Thus, the increasing crystallinity can be a factor, which leads to an increasing of Young's modulus and strength of the reinforced films. The electrostatic interactions between the negatively charged CNC surface (see results for zeta potential in "Preparation of CNC" section) and the positively charged  $-\text{NH}_3^+$  groups of CS can be expected. The positive charge on CS is due to its interaction with MA, which is a component of plasticizer. Additionally, the FTIR spectra (Fig. 5f) demonstrate a slight shift of the cellulose bands near  $1055$  and  $1031\text{ cm}^{-1}$ , which suggest interactions between the  $-\text{OH}$  groups of CNC and the components of the matrix CS/DES film. These factors can lead to the formation of a network of CS-CNC interactions resulting in an increased elongation at break. The same mechanism of CNC reinforcing effect on the CS based film was reported recently (Mao et al. 2019).

Further increase in the CNC content from 2 wt% up to 6 wt% in the CS/CNC-6 sample leads to the increased elongation at break up to 91% accompanied with a slight decrease in the Young's modulus and

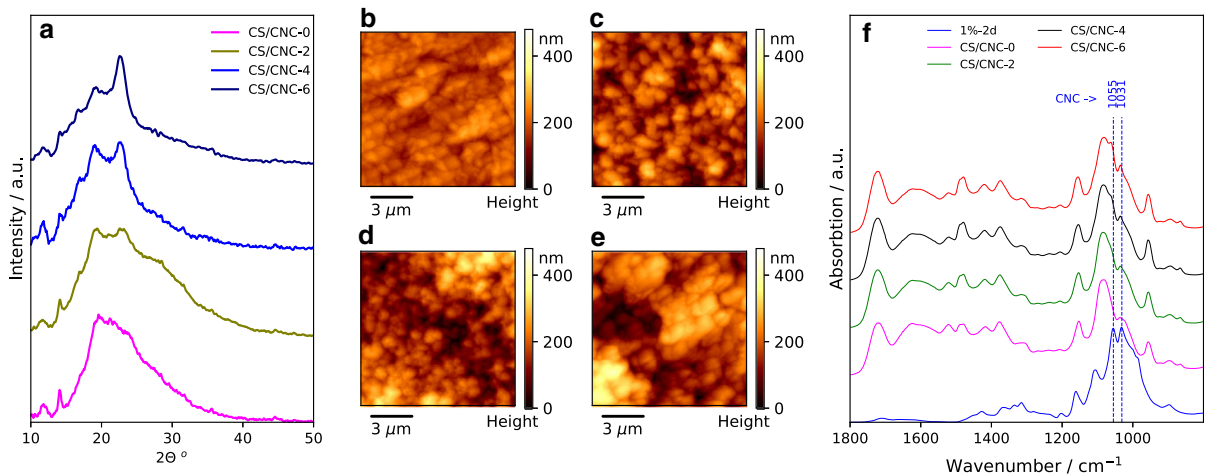


**Fig. 5** WAXD patterns for initial and reinforced films (a); surface map topography for CS/CNC-0 (b), CS/CNC-2 (c), CS/CNC-4 (d), CS/CNC-6 (e) and FTIR spectra for CNC, unmodified and reinforced films (f)

strength. The decrease can be attributed to the less homogenous of CNC distribution in the films, which can be proposed from the increasing of roughness ( $R_q$ ) measured with AFM of film's surface (Fig. 5b-e). The values of  $R_q$  for CS/CNC-0 film was 25 nm, while for composite films the  $R_q$  values were 53, 67 and 75 nm for CS/CNC-2, CS/CNC-4 and CS/CNC-6, respectively.

## Conclusions

A green method for transforming microcrystalline cellulose (MCC) into nanocrystalline cellulose based on the treatment by a deep eutectic solvent (DES) was described. Unlike the classical methods (based on the acid treatment) the developed method allows to obtain cellulose nanocrystals (CNC) without a significant chemical surface modification. This potentially widens the CNC application field and simplifies further treatment of CNC. The molecular mechanism of cellulose solvation in DES was revealed. Molecular dynamics simulations demonstrated that the hydrogen bond interactions of the cellulose hydroxyl groups with the urea C = O group and the chloride ions are the key factors for the destruction of MCC particles in the process of solvation. The crystal structure of cellulose ( $I_\beta$ ) and its high degree of crystallinity remained unchanged during treatment with DES. CNC prepared in this work show a significant reinforcing effect for the chitosan-based films plasticized with DES.

Introduction of 2 wt% of CNC leads to an increase in the strength of the films from 11.4 up to 20.4 MPa with a simultaneous increase in the elongation at break.

**Acknowledgments** Preparation and study of cellulose nanocrystals and molecular dynamic simulations were conducted with a financial support of Russian Ministry of Education and Science within State Contract 14.W03.31.0014 (megagrant). The experimental work was facilitated by the equipment of the Resource Centre for X-ray Diffraction Studies, Centre for Microscopy and Microanalysis, Thermogravimetric and Calorimetric Research Centre, Centre for Optical and Laser Materials Research and Interdisciplinary Resource Centre for Nanotechnology at Saint Petersburg State University and by the Engineering Center of the Saint-Petersburg State Technological Institute (Technical University). Calculations were performed with the use of the resources of the Institute of Macromolecular Compounds and the resources of the Center of collective use "Complex of modelling and data research mega-class facilities" NRC "Kurchatov Institute". Unique identifier RFMEFI62114X0006.

## Compliance with ethical standards

**Conflict of interest** The authors declare that they have no conflict of interest.

## References

- Abraham MJ, Murtola T, Schulz R et al (2015) GROMACS: high performance molecular simulations through multi-level parallelism from laptops to supercomputers. *SoftwareX* 1–2:19–25. <https://doi.org/10.1016/J.SOFTX.2015.06.001>

- Amde M, Liu J-F, Pang L (2015) Environmental application, fate, effects, and concerns of ionic liquids: a review. *Environ Sci Technol* 49:12611–12627. <https://doi.org/10.1021/acs.est.5b03123>
- Amin KNM, Annamalai PK, Morrow IC, Martin D (2015) Production of cellulose nanocrystals via a scalable mechanical method. *RSC Adv* 5:57133–57140. <https://doi.org/10.1039/C5RA06862B>
- Armelin E, Pérez-Madriral MM, Alemán C, Diaz DD (2016) Current status and challenges of biohydrogels for applications as supercapacitors and secondary batteries. *J Mater Chem A* 4:8952–8968. <https://doi.org/10.1039/C6TA01846G>
- Bai W, Holbery J, Li K (2009) A technique for production of nanocrystalline cellulose with a narrow size distribution. *Cellulose* 16:455–465. <https://doi.org/10.1007/s10570-009-9277-1>
- Bajkacz S, Adamek J (2017) Evaluation of new natural deep eutectic solvents for the extraction of isoflavones from soy products. *Talanta* 168:329–335. <https://doi.org/10.1016/j.talanta.2017.02.065>
- Cao L, Yuan D, Fu X, Chen Y (2018) Green method to reinforce natural rubber with tunicate cellulose nanocrystals via one-pot reaction. *Cellulose* 25:4551–4563. <https://doi.org/10.1007/s10570-018-1877-1>
- Chi K, Catchmark JM (2018) Improved eco-friendly barrier materials based on crystalline nanocellulose/chitosan/carboxymethyl cellulose polyelectrolyte complexes. *Food Hydrocoll* 80:195–205. <https://doi.org/10.1016/j.foodhyd.2018.02.003>
- Decaen P, Rolland-Sabaté A, Guilois S et al (2017) Choline chloride vs choline ionic liquids for starch thermoplasticization. *Carbohydr Polym* 177:424–432. <https://doi.org/10.1016/j.carbpol.2017.09.012>
- Deng F, Li M-C, Ge X et al (2017) Cellulose Nanocrystals/poly(methyl methacrylate) nanocomposite films: effect of preparation method and loading on the optical, thermal, mechanical, and gas barrier properties. *Polym Compos* 38:E137–E146. <https://doi.org/10.1002/pc.23875>
- dos Santos FA, Iulianelli GCV, Tavares MIB (2017) Effect of microcrystalline and nanocrystals cellulose fillers in materials based on PLA matrix. *Polym Test* 61:280–288. <https://doi.org/10.1016/j.polymertesting.2017.05.028>
- Essmann U, Perera L, Berkowitz ML et al (1995) A smooth particle mesh Ewald method. *J Chem Phys* 103:8577–8593. <https://doi.org/10.1063/1.470117>
- Feng Q, Hou D, Zhao Y et al (2014) Electrospun regenerated cellulose nano fibrous membranes surface-grafted with polymer chains/brushes via the atom transfer radical polymerization method for catalase immobilization. *ACS Appl Mater Interfaces* 6:20958–20967. <https://doi.org/10.1021/am505722g>
- French AD (2014) Idealized powder diffraction patterns for cellulose polymorphs. *Cellulose* 21:885–896. <https://doi.org/10.1007/s10570-013-0030-4>
- French AD, Santiago Cintrón M (2013) Cellulose polymorphy, crystallite size, and the Segal Crystallinity Index. *Cellulose* 20:583–588. <https://doi.org/10.1007/s10570-012-9833-y>
- Galvis-Sánchez A, Sousa AMM, Hilliou L et al (2016) Thermo-compression molding of chitosan with a deep eutectic mixture for biofilms development. *Green Chem* 18:1571–1580. <https://doi.org/10.1039/C5GC02231B>
- Hirota M, Tamura N, Saito T, Isogai A (2010) Water dispersion of cellulose II nanocrystals prepared by TEMPO-mediated oxidation of mercerized cellulose at pH 4.8. *Cellulose* 17:279–288. <https://doi.org/10.1007/s10570-009-9381-2>
- Hoover WG (1985) Canonical dynamics: equilibrium phase-space distributions. *Phys Rev A* 31:1695–1697. <https://doi.org/10.1103/PhysRevA.31.1695>
- Kabanov VA (ed) (1977) Enciklopedija polimerov, vol 3. Sovetskaya Encyclopedia, Moscow
- Kony D, Damm W, Stoll S, Van Gunsteren WF (2002) An improved OPLS-AA force field for carbohydrates. *J Comput Chem* 23:1416–1429. <https://doi.org/10.1002/jcc.10139>
- Kostritskii AY, Tolmachev DA, Lukasheva NV, Gurtovenko AA (2017) Molecular-level insight into the interaction of phospholipid bilayers with cellulose. *Langmuir* 33:12793–12803. <https://doi.org/10.1021/acs.langmuir.7b02297>
- Lee CM, Kubicki JD, Fan B et al (2015) Hydrogen-bonding network and OH stretch vibration of cellulose: comparison of computational modeling with polarized IR and SFG spectra. *J Phys Chem B* 119:15138–15149. <https://doi.org/10.1021/acs.jpcc.5b08015>
- Leung ACW, Hrapovic S, Lam E et al (2011) Characteristics and properties of carboxylated cellulose nanocrystals prepared from a novel one-step procedure. *Small* 7:302–305. <https://doi.org/10.1002/sml.201001715>
- Li J, Wei X, Wang Q et al (2012) Homogeneous isolation of nanocellulose from sugarcane bagasse by high pressure homogenization. *Carbohydr Polym* 90:1609–1613. <https://doi.org/10.1016/j.carbpol.2012.07.038>
- Li X, Feng Y, Chu G et al (2018) Directly and quantitatively studying the interfacial interaction between SiO<sub>2</sub> and elastomer by using peak force AFM. *Compos Commun* 7:36–41. <https://doi.org/10.1016/j.coco.2017.12.006>
- Ling Z, Edwards JV, Guo Z et al (2019) Structural variations of cotton cellulose nanocrystals from deep eutectic solvent treatment: micro and nano scale. *Cellulose* 26:861–876. <https://doi.org/10.1007/s10570-018-2092-9>
- Liu Y, Guo B, Xia Q et al (2017) Efficient cleavage of strong hydrogen bonds in cotton by deep eutectic solvents and facile fabrication of cellulose nanocrystals in high yields. *ACS Sustain Chem Eng*. <https://doi.org/10.1021/acssuschemeng.7b00954>
- Lukasheva NV, Tolmachev DA (2016) Cellulose nanofibrils and mechanism of their mineralization in biomimetic synthesis of hydroxyapatite/native bacterial cellulose nanocomposites: molecular dynamics simulations. *Langmuir* 32:125–134. <https://doi.org/10.1021/acs.langmuir.5b03953>
- Lynam JG, Kumar N, Wong MJ (2017) Deep eutectic solvents' ability to solubilize lignin, cellulose, and hemicellulose; thermal stability; and density. *Bioresour Technol*. <https://doi.org/10.1016/j.biortech.2017.04.079>
- Man Z, Muhammad N, Sarwono A et al (2011) Preparation of cellulose nanocrystals using an ionic liquid. *J Polym Environ* 19:726–731. <https://doi.org/10.1007/s10924-011-0323-3>

- Mao H, Wei C, Gong Y et al (2019) Mechanical and water-resistant properties of eco-friendly chitosan membrane reinforced with cellulose nanocrystals. *Polym (Basel)* 11:166. <https://doi.org/10.3390/polym11010166>
- Maréchal Y, Chanzy H (2000) The hydrogen bond network in I<sub>β</sub> cellulose as observed by infrared spectrometry. *J Mol Struct* 523:183–196. [https://doi.org/10.1016/S0022-2860\(99\)00389-0](https://doi.org/10.1016/S0022-2860(99)00389-0)
- Marín-Silva DA, Rivero S, Pinotti A (2019) Chitosan-based nanocomposite matrices: development and characterization. *Int J Biol Macromol* 123:189–200. <https://doi.org/10.1016/j.ijbiomac.2018.11.035>
- Miao J, Yu Y, Jiang Z, Zhang L (2016) One-pot preparation of hydrophobic cellulose nanocrystals in an ionic liquid. *Cellulose* 23:1209–1219. <https://doi.org/10.1007/s10570-016-0864-7>
- Mondal S (2017) Preparation, properties and applications of nanocellulosic materials. *Carbohydr Polym* 163:301–316. <https://doi.org/10.1016/j.carbpol.2016.12.050>
- Mostofian B, Smith JC, Cheng X (2014) Simulation of a cellulose fiber in ionic liquid suggests a synergistic approach to dissolution. *Cellulose* 21:983–997. <https://doi.org/10.1007/s10570-013-0018-0>
- Mukesh C, Mondal D, Sharma M, Prasad K (2014) Choline chloride-thiourea, a deep eutectic solvent for the production of chitin nanofibers. *Carbohydr Polym* 103:466–471. <https://doi.org/10.1016/j.carbpol.2013.12.082>
- Nosé S (1984) A molecular dynamics method for simulations in the canonical ensemble. *Mol Phys* 52:255–268. <https://doi.org/10.1080/00268978400101201>
- Parrinello M, Rahman A (1981) Polymorphic transitions in single crystals: a new molecular dynamics method. *J Appl Phys* 52:7182–7190. <https://doi.org/10.1063/1.328693>
- Ren H, Chen C, Wang Q et al (2016) The properties of choline chloride-based deep eutectic solvents and their performance in the dissolution of cellulose. *BioResources* 11:5435–5451. <https://doi.org/10.15376/biores.11.2.5435-5451>
- Rovera C, Ghaani M, Santo N et al (2018) Enzymatic hydrolysis in the green production of bacterial cellulose nanocrystals. *ACS Sustain Chem Eng* 6:7725–7734. <https://doi.org/10.1021/acssuschemeng.8b00600>
- Samarov AA, Smirnov MA, Sokolova MP, Toikka AM (2018a) Liquid–liquid equilibrium data for the system N-Octane + Toluene + DES at 293.15 and 313.15 K and atmospheric pressure. *Theor Found Chem Eng* 52:262–267. <https://doi.org/10.1134/S0040579518020148>
- Samarov AA, Smirnov MA, Toikka AM, Prikhodko IV (2018b) Study of deep eutectic solvent on the base choline chloride as entrainer for the separation alcohol-ester systems. *J Chem Eng Data* 63:1877–1884. <https://doi.org/10.1021/acs.jced.7b00912>
- Sambasivarao SV, Acevedo O (2009) Development of OPLS-AA force field parameters for 68 unique ionic liquids. *J Chem Theory Comput* 5:1038–1050. <https://doi.org/10.1021/ct900009a>
- Segal L, Creely JJ, Martin AE, Conrad CM (1959) An empirical method for estimating the degree of crystallinity of native cellulose using the X-Ray diffractometer. *Text Res J* 29:786–794. <https://doi.org/10.1177/004051755902901003>
- Sirviö JA, Visanko M, Liimatainen H (2015) Deep eutectic solvent system based on choline chloride-urea as a pre-treatment for nanofibrillation of wood cellulose. *Green Chem* 17:3401–3406. <https://doi.org/10.1039/C5GC00398A>
- Sirviö JA, Visanko M, Liimatainen H (2016) Acidic Deep eutectic solvents as hydrolytic media for cellulose nanocrystal production. *Biomacromolecules* 17:3025–3032. <https://doi.org/10.1021/acs.biomac.6b00910>
- Smirnov MA, Vorobiov VK, Sokolova MP et al (2018) Electrochemical properties of supercapacitor electrodes based on polypyrrole and enzymatically prepared cellulose nanofibers. *Polym Sci Ser C* 60:228–239. <https://doi.org/10.1134/S1811238218020194>
- Smith EL, Abbott AP, Ryder KS (2014) Deep eutectic solvents (DESs) and their applications. *Chem Rev* 114:11060–11082. <https://doi.org/10.1021/cr300162p>
- Sokolova MP, Smirnov MA, Samarov AA et al (2018) Plasticizing of chitosan films with deep eutectic mixture of malonic acid and choline chloride. *Carbohydr Polym* 197:548–557. <https://doi.org/10.1016/j.carbpol.2018.06.037>
- Sun H, Li Y, Wu X, Li G (2013) Theoretical study on the structures and properties of mixtures of urea and choline chloride. *J Mol Model* 19:2433–2441. <https://doi.org/10.1007/s00894-013-1791-2>
- Suopajarvi T, Sirviö JA, Liimatainen H (2017) Nanofibrillation of deep eutectic solvent-treated paper and board cellulose pulps. *Carbohydr Polym* 169:167–175. <https://doi.org/10.1016/j.carbpol.2017.04.009>
- Surov OV, Voronova MI, Afineevskii AV, Zakharov AG (2018a) Polyethylene oxide films reinforced by cellulose nanocrystals: microstructure-properties relationship. *Carbohydr Polym* 181:489–498. <https://doi.org/10.1016/j.carbpol.2017.10.075>
- Surov OV, Voronova MI, Rubleva NV et al (2018b) A novel effective approach of nanocrystalline cellulose production: oxidation–hydrolysis strategy. *Cellulose* 25:5035–5048. <https://doi.org/10.1007/s10570-018-1910-4>
- Tang J, Berry RM, Tam KC (2016) Stimuli-responsive cellulose nanocrystals for surfactant-free oil harvesting. *Biomacromolecules* 17:1748–1756. <https://doi.org/10.1021/acs.biomac.6b00144>
- Tenhunen T-M, Lewandowska AE, Orelma H et al (2018) Understanding the interactions of cellulose fibres and deep eutectic solvent of choline chloride and urea. *Cellulose* 25:137–150. <https://doi.org/10.1007/s10570-017-1587-0>
- Trotter DZ, Todorović ZB, Đokić-Stojanović DR et al (2016) Application of ionic liquids and deep eutectic solvents in biodiesel production: a review. *Renew Sustain Energy Rev* 61:473–500
- Wang Y, Wang X, Xie Y, Zhang K (2018) Functional nanomaterials through esterification of cellulose: a review of chemistry and application. *Cellulose* 25:3703–3731. <https://doi.org/10.1007/s10570-018-1830-3>
- Weerasinghe S, Smith PE (2003) A Kirkwood–Buff derived force field for sodium chloride in water. *J Phys Chem B* 119:3891–3898
- Wu W, Huang F, Pan S et al (2015) Thermo-responsive and fluorescent cellulose nanocrystals grafted with polymer

- brushes. *J Mater Chem A Mater energy Sustain* 3:1995–2005. <https://doi.org/10.1039/C4TA04761C>
- Ying Z, Wu D, Wang Z et al (2018) Rheological and mechanical properties of polylactide nanocomposites reinforced with the cellulose nanofibers with various surface treatments. *Cellulose* 25:3955–3971. <https://doi.org/10.1007/s10570-018-1862-8>
- Zainal-Abidin MH, Hayyan M, Hayyan A, Jayakumar NS (2017) New horizons in the extraction of bioactive compounds using deep eutectic solvents: a review. *Anal Chim Acta* 979:1–23. <https://doi.org/10.1016/j.aca.2017.05.012>
- Zhang Q, Vigier KDO, Royer S, Jerome R (2012) Deep eutectic solvents: syntheses, properties and applications. *Chem Soc Rev* 41:7108–7146. <https://doi.org/10.1039/c2cs35178a>
- Zhou Y, Saito T, Bergström L, Isogai A (2018) Acid-free preparation of cellulose nanocrystals by TEMPO oxidation and subsequent cavitation. *Biomacromolecules* 19:633–639. <https://doi.org/10.1021/acs.biomac.7b01730>
- Zhu P, Gu Z, Hong S, Lian H (2017) One-pot production of chitin with high purity from lobster shells using choline chloride–malonic acid deep eutectic solvent. *Carbohydr Polym* 177:217–223. <https://doi.org/10.1016/j.carbpol.2017.09.001>

**Publisher's Note** Springer Nature remains neutral with regard to jurisdictional claims in published maps and institutional affiliations.